

Spatiotemporal Tracking of Persistent, Localized Speckles in Turbulent Atmospheric Propagation

Travis M. Crumpton* and Luat T. Vuong†

Department of Physics and Astronomy, University of California at Riverside, Riverside, CA, 92521 USA

Department of Electrical and Computer Engineering,

University of California at Riverside, Riverside, CA, 92521 USA and

Department of Mechanical Engineering, University of California at Riverside, Riverside, CA, 92521 USA

Light propagation through turbulence produces speckles, whose ensemble behavior is typically characterized by snapshot intensity statistics. Here, we track the spatiotemporal evolution of individual speckles and quantify fragmentation, localization, and persistence under different diffraction and turbulence scales. Beam fragmentation coincides with complete spatial decorrelation defined by the magnitude-squared coherence. Fragmentation occurs closer to the source for larger beams, which indicates that smaller beams are more robust to decoherence. Subsequently, speckles are both spatially localized and persistent over distances significantly longer than their associated Rayleigh length. The combination of localization and persistence impacts the statistics of light relevant to their long-distance signaling and sensing.

I. INTRODUCTION

Speckle fields arise when a coherent electromagnetic wave encounters random phase or amplitude modulations imposed by rough surfaces or inhomogeneous media such as atmospheric or oceanic environments [1–4]. The first- and second-order ensemble statistics [5–10], spatiotemporal correlations [11, 12], and phase-singularity structures [13, 14] have previously been established and extensively studied. Prior literature treats the speckle fields as a wide-sense stationary random field and emphasizes speckle intensity distributions, spatial correlation functions, and singularity densities rather than tracking any particular features. While it is known that the time evolution of the speckle fields identify characteristics about the intermediate medium [15, 16], the spatiotemporal dynamics of individual speckles have not, to our knowledge, been systematically studied.

In practice, speckle is viewed either as wavefront distortions that require corrective filtering or adaptive optics or as features that carry information. For imaging and metrology, speckle is suppressed to recover underlying structure [17–19], whereas others use speckle statistics or phase-singularity patterns to characterize the medium or the field itself [14–16, 20–24]. Generally, the primary focus is on the ensemble statistics that capture trends via the scintillation index σ_I^2 , log-amplitude/phase structure functions, and correlation lengths. The statistics do not reflect the individual object-level characteristics exemplified by the speckles themselves.

Here, we examine the speckle structures that emerge during turbulent beam propagation and study the signatures associated with transverse optical localization. The observation of temporally persistent, non-Rayleigh non-diffracting speckle structures [25] motivates the comparison to Anderson localization in disordered dielectric media, where multiple scattering and interference confine the optical energy transversely [26–32]. We track the individual speckles that are produced during propagation, quantifying their widths, trajectories, creation and disappearance events and lifetimes. We monitor these behaviors as the beam evolves through the weak turbulence regime, the focusing regime, and into the saturation regime [8–10]. The parameters that we study are the inner scale ℓ_0 and the beam width w_0 . The outer scale L_0 and the power spectral density may also contribute to the onset of localization and persistence but are not studied here. This object-level view complements established ensemble statistics [5–7, 9, 11–14] and provides a framework for the discrete statistics of speckle, which individually behave like transverse-localized states in disordered dielectrics [25–31]. Our results point to the local sampling and partial sensing of light beams, knowledge of which is vital for building long-distance, free-space optical systems in atmospheric and oceanic environments.

II. THEORY

Electromagnetic wave propagation in turbulent media is described by the inhomogeneous paraxial wave equation [33]:

$$\nabla_{\perp}^2 U + 2ik \frac{\partial U}{\partial z} + 2k^2 \delta n(x, y, z) U = 0. \quad (1)$$

where $k = 2\pi n_0 / \lambda$, n_0 is the background refractive index, $\nabla_{\perp}^2 = \frac{\partial^2}{\partial x^2} + \frac{\partial^2}{\partial y^2}$, $\delta n(x, y, z)$ is the change in refractive index from n_0 , and U is the complex-valued amplitude of the electric field. Eq. 1 is numerically modeled using split step propagation with the Fresnel transfer function as discussed in [34]. The modified von Kármán power spectrum is used here to model the stochastic fluctuations

* tcrum001@ucr.edu

† luatv@ucr.edu

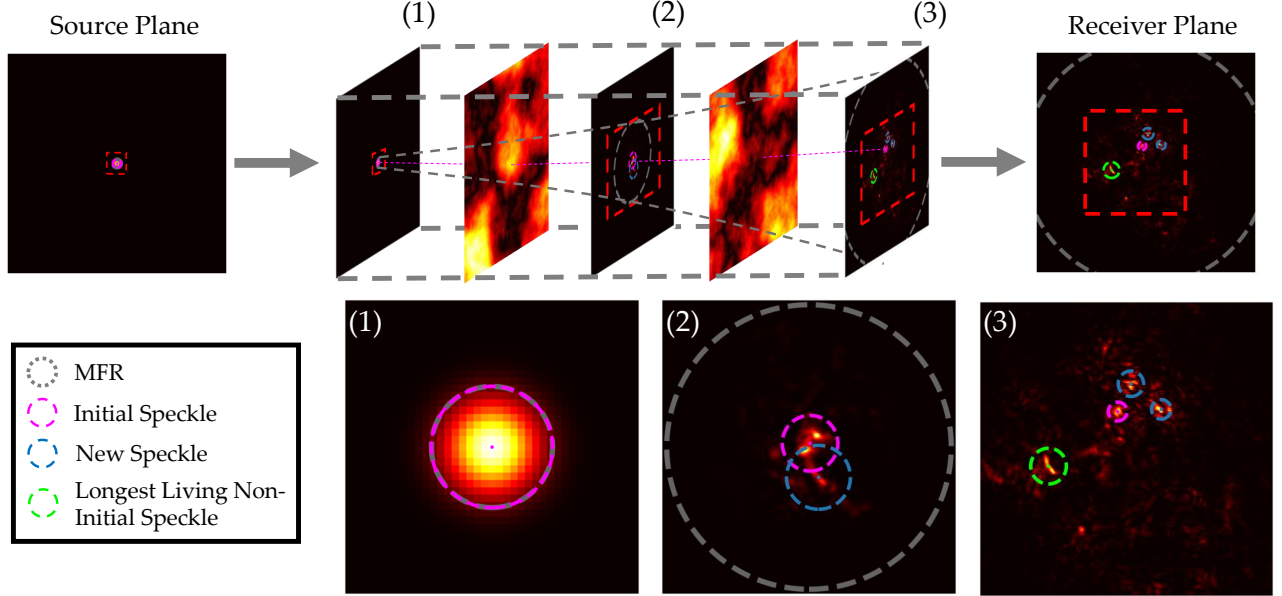


FIG. 1. Speckle simulation and tracking. Top row: spatial beam profiles from the source plane to the receiver plane with representative turbulence profiles. The mode field radius $\tilde{r}(z)$ (gray), source plane speckle (magenta), longest lived non-initial speckle (green), and other detected speckles (blue) are tracked based on their nearest neighbor conditions. Bottom row: magnified views (red box) of observation points (1-3). Detected structures have a local peak intensity greater than ηI_{\max} .

in the refractive index:

$$\Phi_n(\kappa) = 0.033 C_n^2 (\kappa^2 + k_0^2)^{-11/6} \exp\left(-\frac{\kappa^2}{k_m^2}\right) \quad (2)$$

where κ is the transverse spatial frequency. The parameters $k_0 = 2\pi/L_0$ and $k_m = 5.92/\ell_0$ represent the low- and high-wavenumber cutoffs corresponding to the outer and inner scales of turbulence, respectively, while C_n^2 is the refractive-index structure parameter. The power spectral density is the Fourier transform of the spatial covariance of the refractive index perturbations.

The perturbations introduced by the turbulence produce intensity fluctuation known as scintillation, which is analytically discussed in [8, 35] and statistically represented by:

$$\sigma_I^2 = \frac{E[I^2] - E[I]^2}{E[I]^2}. \quad (3)$$

Here, $I = |U(x, y, z)|^2$ is the intensity and σ_I^2 is a measure of the intensity fluctuations within the profile [36]. These perturbations induce filamentation [30], indicative of branched flow behavior [37], which guides light through the random medium. Transverse optical trapping and speckle formation occurs when light is propagated through these branches. This process is associated with the focusing regime of the scintillation index where random focusing consolidates power into speckles [10]. The mean radius of a speckle filament decreases with increasing turbulence strength and can be used to infer C_n^2 . The average size of the speckles produced are associated

with the Fried parameter defined by [9, 10, 38] as:

$$r_0 = \left[0.423k^2 \int_0^L C_n^2(z') dz' \right]^{-3/5}. \quad (4)$$

which itself is related to the spatial coherence radius discussed in [10].

A. Speckle Tracking

We depart from the ensemble analysis with an intensity-based speckle detection and tracking algorithm and report four complementary diagnostics per beam propagation realization:

- (i) Global beam mode field radius (MFR) $\tilde{r}(z)$
- (ii) Global beam spatial correlation $\mathcal{C}(z)$
- (iii) Persistence Δz_j of each individual speckle denoted by the subscript j
- (iv) Speckle confinement $\tilde{r}_j(z)$.

Each speckle is determined by an intensity threshold criteria and a radius threshold criteria. The intensity threshold is defined as ηI_{\max} where η is related to a detector's sensitivity and I_{\max} is the global intensity maximum in the source plane. Here, $\eta = 0.01$ representing a detector whose sensitivity is one percent of the maximum initial intensity. Adjacent or collocated speckles

are removed and filtered from the analysis if their location is within a radius threshold. This prevents multiple speckle detections within regions of high intensity. Fig. 1 illustrates this tracking algorithm at three different observation points with colored tracking circles showing the temporal stability of speckles.

B. Spatial Coherence $\mathcal{C}(z)$

The observed fragmentation, or rapid, stochastic increase in the number of speckles, coincides with the gradual breakdown of global coherence across the beam cross-section. This indicates phase change-like behavior with rising turbulence strength as the beam approaches the focusing regime. While the global MFR,

$$\tilde{r}(z) = \frac{\sqrt{2 \iint (x^2 + y^2) |U(x, y, z)|^2 dx dy}}{\sqrt{\iint |U(x, y, z)|^2 dx dy}}, \quad (5)$$

quantifies the overall spatial spread of energy, it does not reveal how the phase and amplitude correlations evolve during propagation.

To assess the onset of spatial decoherence and its relation to speckle formation, we evaluate the cross-correlation between the vacuum-propagated field $U_{\text{vac}}(x, y, z)$ and turbulence-propagated field $U_{\text{turb}}(x, y, z)$. We quantify the loss of spatial coherence with the normalized complex field overlap, or magnitude-squared coherence, between the vacuum-propagated field and the turbulence-propagated, centroid-aligned field [39, 40],

$$\mathcal{C}(z) = \frac{|\iint U_{\text{vac}}^* U_{\text{turb}} dx dy|^2}{(\iint |U_{\text{vac}}|^2 dx dy)(\iint |U_{\text{turb}}|^2 dx dy)}. \quad (6)$$

This provides a direct statistical measure of the remaining degree of *global order* as stochastic fluctuations accumulate. At each observation plane, the turbulence-propagated field is re-centered by its intensity centroid to remove beam wander before the correlation is evaluated. The transition from complete spatial coherence to a completely decorrelated beam marks the onset of stochastic focusing and beam fragmentation.

C. Speckle Localization $\tilde{r}(z)$ and Persistence Δz_j

Previous studies have identified that light interacting with strong distortions induced by a dielectric medium can exhibit localization[29, 31, 41, 42]. Generally, Anderson localization is achieved via multiple scattering and diffraction in static, time-independent disordered media. In contrast, in a time-varying stochastic medium where the refractive index varies as a function of propagation, these effects are diluted into a form of partial localization, where only subsections of the beam exhibit localization.

Confinement and persistence refer to the spatial and temporal conditions associated with stable transverse speckle localization. Confinement, $\tilde{r}_j(z)$, is the average radius of the $1/e^2$ contour of the j th speckle. Persistence, Δz_j , quantifies the temporal continuity of the j th structure during propagation. This framework for speckle analysis is similar to other tracking methods applied to study optical phase singularities [13, 14]. We define persistence Δz_j as the propagation distance between creation and disappearance events identified by the intensity and radius thresholds. We compare Δz_j to its associated diffraction length $z_{0,j} = \pi w_{0,j}^2 / \lambda$ where $w_{0,j}$ is the initial width of the j th speckle at time of creation. We bin each speckle according to $\Delta z_j/z_{0,j}$ and generate a distribution that describes the probability of finding a speckle that persists past their associated diffraction length.

III. RESULTS AND DISCUSSION

A. Mode Field Radius $\tilde{r}(z)$

The global MFR trend in Fig. 2 does not reveal localization, as conventionally explored [29–31]; there is no global confinement to the beam. However, within the expanding beam, speckle fragments occur, and as the turbulence strength increases, a greater number of smaller fragments are observed with their initial onset approaching closer to the source plane. Fragmentation dependence on C_n^2 is further visualized by the right panels (a1–a4, b1–b4, c1–c4) of Fig. 2 which show the transverse profiles located at varying distances from the source plane.

The speckle spatial distribution is confined within the MFR. Energy consolidation into a detectable speckle becomes more difficult as the distance from the center of the beam increases due to the drop off in power. Spatially, the probability of observing a speckle follows a gaussian distribution which reflects the the long-exposure statistics of a Gaussian beam, indicating that energy remains statistically confined within the global MFR. The earlier onset of fragments with higher C_n^2 suggest a progressive loss of spatial beam coherence.

B. Spatial Correlation $\mathcal{C}(z)$

As the beam propagates through turbulence, stochastic phase distortions accumulate, progressively reducing spatial correlation and breaking the field into localized speckles. In Fig. 3, we compare the evolution of $\mathcal{C}(z)$ computed from Eq. 6 with the theoretical plane-wave scintillation index σ_I^2 . Both quantities are plotted as functions of the propagation distance z and Rytov parameter $\sigma_R = \sqrt{1.23 C_n^2 k^{7/6} L^{11/6}}$.

With increasing C_n^2 , the decay of $\mathcal{C}(z)$ changes from a gradual, sigmoid-like drop off to an approximately exponential decline with distance. Complete spatial decor-

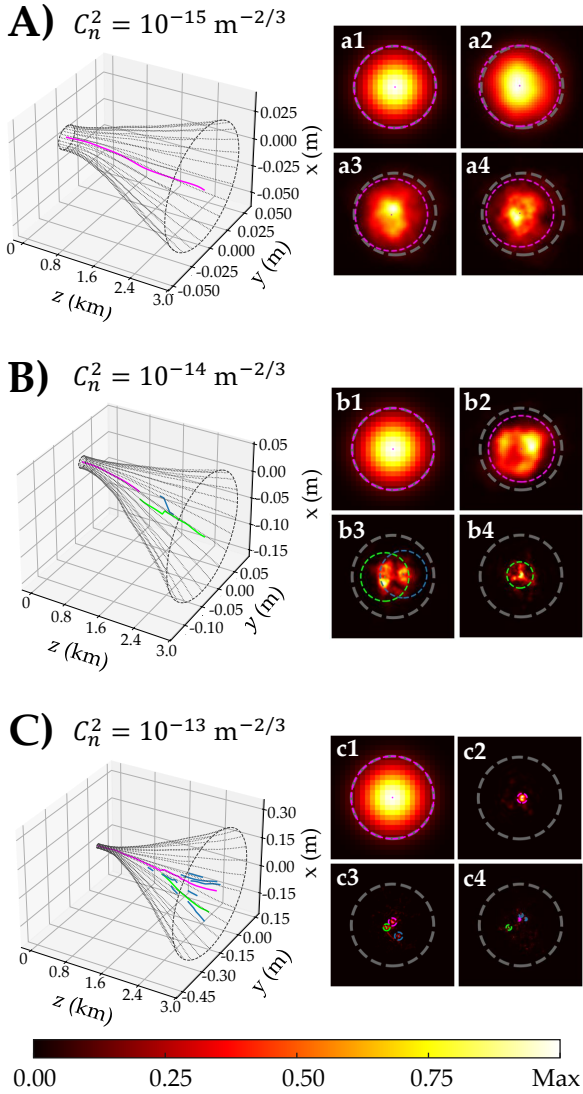


FIG. 2. Propagation of Gaussian profiles under (A) weak turbulence ($\sigma_R^2 = 0.558$), (B) moderately-strong turbulence ($\sigma_R^2 = 5.58$), and (C) strong turbulence ($\sigma_R^2 = 55.8$). The transverse profiles (a1-a4, b1-b4, c1-c4) show the width evolution of the MFR (gray) and speckles (magenta, lime, blue) for the same realizations shown in the trajectory plots on the left located at $z = 0, 975, 1950, 3000$ m. Conditions: $w_0 = 1$ cm and $\ell_0 = 5$ mm.

relation is defined as $\mathcal{C}(z = L_c) \approx 0.01$ where L_c is the decorrelation distance. This occurs near $\sigma_R \approx 4$, corresponding to $z \approx 1500$ m for $C_n^2 = 10^{-13} \text{ m}^{-2/3}$ and can be identified by an increase in the number of identified speckles N_{speckles} . The trajectory plots in Fig. 3(B-E) are single representative realizations for the same parameter sets used in Fig. 3A. The primary and ancillary speckle trajectories are denoted by the same color scheme used in Fig. 1. The earlier onset of fragmentation seen in plots (B) and (D) coincide earlier decorrelation, increased fragmentation, and wider speckle spatial distribution.

Variations in the inner scale ℓ_0 produce differences in the measured spatial correlation and substantially alter the theoretical σ_I^2 . ℓ_0 primarily truncates high-wavenumber components of the refractive-index power spectrum, suppressing small-scale intensity fluctuations while leaving the large-scale phase correlations largely unaffected. The correlation metric is thus governed mainly by low-spatial-frequency structure rather than by fine speckle granularity. Beyond this distance of complete decorrelation, the beam no longer behaves as a coherent optical mode but as a collection of statistically independent speckles. In other words, past the decorrelation distance the dynamics are less dependent on the initial beam parameters.

Larger beams exhibit faster decorrelation due to their wider sampling of turbulent inhomogeneities, which explains the offset between red and blue curves in Fig. 3. Increasing the size of the beam decreases the spatial frequency of the beam, $k_{\text{beam}} = 2\pi/w_0$, and increases its sensitivity to low-frequency components of the refractive-index power spectrum. Consequently, larger beams experience stronger cumulative phase distortions over shorter distances, resulting in earlier loss of spatial coherence and more rapid fragmentation. In contrast, smaller beams exhibit greater resilience to low-order distortions and maintain partial coherence over a longer propagation range.

C. Speckle Localization and Persistence

Figure 4 shows the width fluctuations of all detected speckles in a single realization as compared to the statistics gathered for the initial identified speckle and global beam envelope across 500 runs. In the presence of strong turbulence, the average width of the initial speckle $\tilde{r}_0(z)$ approaches approximately $1.7w_0$ when $C_n^2 = 10^{-13} \text{ m}^{-2/3}$ where w_0 is the global beam spot size. Other speckles fall within this range of width statistics as well, indicating that the width evolution of the initial speckle statistically represents the ensemble behavior of other detected speckles.

Undulations in $\tilde{r}_j(z)$ occur as a result of scintillation [8–10, 43], which has been shown to be minimized with the use of partially coherent beams [44, 45], and phase structure [13, 14]. Nonuniform intensity consolidation in the speckle reduces $\tilde{r}_j(z)$ and power reduction expands it. In the absence of turbulence, there are no perturbations in spatial structure or intensity, thus as $C_n^2 \rightarrow 0$, $\tilde{r}_j(z) \rightarrow \tilde{r}(z)$ which itself approaches the analytical solution for the width of a Gaussian beam in vacuum [46] $w(z) = w_0 \sqrt{1 + \left(\frac{z}{z_0}\right)^2}$.

Figure 4(A-C) demonstrates the approach of the initial speckle behavior to the expected behavior of the global beam envelope which itself is approaching the trend described by Gaussian statistics for $w(z)$. In vacuum with a Gaussian beam, the initial profile in the source plane is identified as a speckle, the beam survives the entire prop-

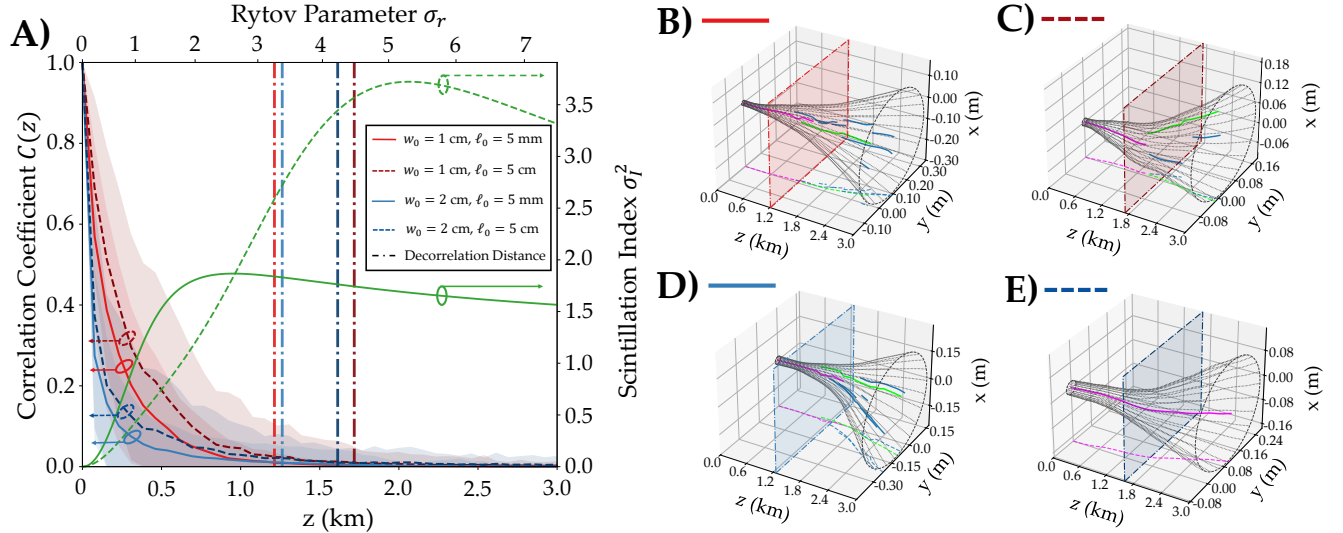


FIG. 3. Transition to speckle fragmentation. (A) Spatial coherence $\mathcal{C}(z)$ (left axis) for varied beam widths w_0 and inner scales ℓ_0 under strong turbulence ($C_n^2 = 10^{-13} \text{ m}^{-2/3}$). The decorrelation distances L_c (vertical lines) loosely correspond with the focusing regime of the scintillation index σ_I^2 (right axis, green), whose analytic relation only depends on ℓ_0 . (B-E) Trajectory plots of representative realizations corresponding to (A). The tracks are projected with dashed lines in the $y - z$ plane. The shaded planes (dashed borders, $z = L_c$) mark the transition to speckle fragmentation.

agation path, and confinement is absent as the speckle expands monotonically with the global beam waist. As C_n^2 increases, persistence decreases and confinement approaches the predicted speckle size associated with the Fried parameter [Eq. 4].

The combination of persistence and confinement enables stable partial localization within substructures of the beam. Confinement without persistence results in unstable localization that occurs under short time scales. Persistence without confinement describes the process of vacuum propagation of a Gaussian beam but the generation of the initial speckle is dependent upon allowable speckle structures that can be identified by the algorithm. Low persistence and low confinement give rise to unstructured fluctuations. The persistence statistics are also a measure of the partial localization stability and which can be seen in the histograms (Fig. 4, inset) and show the distribution of the lifetimes of speckles that did not survive the entire path.

The distribution of normalized persistence $\Delta z_j/z_{0,j}$ reveals how turbulence strength reshapes the lifetime statistics of localized structures. This quantity approaches a negative exponential probability distribution as C_n^2 increases. A high count in the 0.0 bin indicates numerous short-lived or low-power speckles whose large initial radii artificially inflate their associated diffraction length. $C_n^2 = 10^{-13} \text{ m}^{-2/3}$ exhibits the most speckles binned in the 0.0 bin indicating that beams under that level of turbulence generate the most short lived speckles. By contrast, $C_n^2 = 10^{-15} \text{ m}^{-2/3}$ exhibits the least number of speckles binned in the 0.0 bin and the highest number of speckles persisting well past their associated

diffraction lengths.

The number of detected speckles and their average lifetimes exhibit strong, quantifiable scaling with turbulence strength indicating phase change-like behavior. For strong turbulence across 500 iterations, ≈ 4738 speckles were identified with approximately 2% surviving longer than 5 diffraction lengths while 10% propagated at least a single diffraction length. For weak turbulence, ≈ 700 speckles were identified with approximately 66% surviving the entire propagation distance. From weak turbulence to strong turbulence, there is an increase in the total number of speckles N_{speckles} by $7\times$ and the average lifetime decreases by a factor of $4\times$. Strong turbulence therefore produces fewer persistent speckles than weak turbulence. Within the range $C_n^2 = 10^{-15}-10^{-13} \text{ m}^{-2/3}$, the persistence distribution evolves toward a negative exponential form, as shown in Fig. 4(C). This inverse relationship between speckle count and persistence reflects the redistribution of optical energy into smaller, transient substructures under stronger turbulence.

The observed scaling between speckle persistence and turbulence strength suggests that persistence statistics could serve as a diagnostic tool for estimating effective refractive-index structure parameters. The relationship between speckle persistence and turbulence strength could enable the classification of time-averaged effective refractive index structure parameters $\langle C_n^2 \rangle$. This requires short-exposure measurements that capture speckle evolution on the time scale of the turbulent fluctuations and at multiple observation planes. The dependence on observation density can be mitigated by replacing persistence metrics with the time-averaged statistics of the speckle

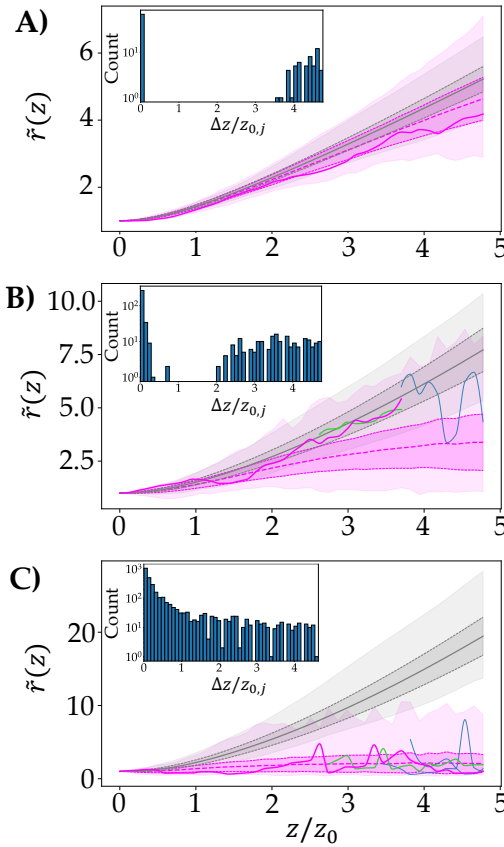


FIG. 4. Evolution of the spot-normalized MFR $\tilde{r}(z)/w_0$ of the global beam (gray) and tracked speckles (magenta, lime, blue) under (A) weak ($\sigma_R^2 = 0.558$), (B) moderately-strong ($\sigma_R^2 = 5.58$), and (C) strong ($\sigma_R^2 = 55.8$) turbulence. The ensemble averages (dashed), standard deviation (shaded dark), and the maxima/minima (shaded light) across all 500 runs show increasing confinement. The inset histograms of the spot-normalized Rayleigh lengths $\Delta z_j/z_{0,j}$ show the transition of persistence statistics from a bimodal to a long-tailed distribution.

count N_{speckles} . Pairing this analysis with observations of speckle confinement can increase the accuracy of the estimation of $\langle C_n^2 \rangle$.

IV. CONCLUSION

As trackable objects rather than anonymous samples of a stationary random field, we observe the persistence of spatially confined speckles multiple diffraction lengths. Their behavior is analogous to Anderson localization, however, they are only partially localized. As a result, the highest degrees of persistence and confinement occur at an intermediate range of diffraction and turbulence parameters. The localization of speckles only occurs after the focusing regime where fragmentation of the beam induces complete spatial decorrelation.

The analysis here opens up potential advancements in discrete classification of continuous fields in optically turbulent systems. Our understanding of speckle statistics offers new approaches to estimate time averaged effective refractive index structure parameters $\langle C_n^2 \rangle$. The spatiotemporal speckle confinement and persistence dynamics reveal the partially localized sensing with free-space optical beams. Such knowledge is relevant to the statistical and deterministic design of sampling and imaging systems not limited to turbulence but in the presence of obstructions or obscurants.

-
- [1] O. Korotkova and L. C. Andrews, in *Laser Radar Technology and Applications VII*, Vol. 4723 (SPIE, 2002) pp. 73–84.
[2] O. Korotkova, L. C. Andrews, and R. L. Phillips, in *Free-Space Laser Communication and Laser Imaging II*, Vol. 4821 (SPIE, 2002) pp. 98–109.
[3] O. Korotkova, N. Farwell, and E. Shchepakina, *Waves in Random and Complex Media* **22**, 260 (2012).
[4] M. Beason, L. Andrews, and S. Gladysz, in *Environmental Effects on Light Propagation and Adaptive Systems II*, Vol. 11153 (SPIE, 2019) pp. 104–120.
[5] M. H. Lee, J. F. Holmes, and J. R. Kerr, *Journal of the Optical Society of America* **66**, 1164 (1976).
[6] J. W. Goodman, *Speckle phenomena in optics: theory and applications* (Roberts and Company Publishers, 2007).
[7] J. W. Goodman, *JOSA* **66**, 1145 (1976).
[8] L. C. Andrews, R. L. Phillips, C. Y. Hopen, and M. Al-Habash, *Journal of the Optical Society of America A* **16**, 1417 (1999).
[9] L. C. Andrews and R. L. Phillips, *Laser Beam Propagation Through Random Media: Second Edition* (2005).
[10] L. C. Andrews and M. K. Beason, *Laser beam propagation in random media: new and advanced topics* (2023).
[11] W. Liguo, G. Lei, L. Yaqing, Y. Zhiqiang, Y. Lihong, and L. Yao, *Heliyon* **9** (2023).
[12] L. I. Goldfischer, *Journal of the optical society of america* **55**, 247 (1965).
[13] O. V. Angelsky, A. P. Maksimyak, P. P. Maksimyak, and S. G. Hanson, *Open Optics Journal* **3**, 29 (2009).
[14] X. Cheng, Y. Lockerman, and A. Z. Genack, *Optics letters* **39**, 3348 (2014).
[15] M. Migliaccio, L. Huang, and A. Buono, *IEEE Transactions on Geoscience and Remote Sensing* **57**, 5447 (2019).

- [16] M. Migliaccio, F. Abbasi, M. Zahribanhesari, G. Inserra, A. Verlanti, and G. Grieco, in *IGARSS 2024-2024 IEEE International Geoscience and Remote Sensing Symposium* (IEEE, 2024) pp. 1773–1776.
- [17] B. Macintosh, L. Poyneer, A. Sivaramakrishnan, and C. Marois, in *Astronomical Adaptive Optics Systems and Applications II*, Vol. 5903 (SPIE, 2005) pp. 170–177.
- [18] N. R. Van Zandt and M. F. Spencer, *Applied Optics* **59**, 1071 (2020).
- [19] S. Gladysz and J. C. Christou, *The Astrophysical Journal* **684**, 1486 (2008).
- [20] S. Guyot, M.-C. Péron, and E. Deléchelle, *Physical Review E—Statistical, Nonlinear, and Soft Matter Physics* **70**, 046618 (2004).
- [21] S. Zhang, B. Hu, P. Sebbah, and A. Z. Genack, *Physical review letters* **99**, 063902 (2007).
- [22] J. Garnier and K. Sølna, *Inverse Problems* **34**, 094003 (2018).
- [23] E. Garcia-Caurel, A. Plyer, E. Colin, X. Orlik, and R. Os-sikovski, *Journal of the Optical Society of America A* **42**, 1531 (2025).
- [24] J. P. Bos, G. Archer, and M. C. Roggemann, in *Laser Communication and Propagation through the Atmosphere and Oceans II*, Vol. 8874 (SPIE, 2013) pp. 162–170.
- [25] R. Liu, B. Qing, S. Zhao, P. Zhang, H. Gao, S. Chen, and F. Li, *Physical review letters* **127**, 180601 (2021).
- [26] A. Lagendijk, B. v. Tiggelen, and D. S. Wiersma, *Physics today* **62**, 24 (2009).
- [27] P. A. Lee and D. S. Fisher, *Physical Review Letters* **47**, 882 (1981).
- [28] R. Gade, *Nuclear Physics B* **398**, 499 (1993).
- [29] M. Segev, Y. Silberberg, and D. N. Christodoulides, *Nature Photonics* **7**, 197 (2013).
- [30] H. De Raedt, A. Lagendijk, and P. de Vries, *Physical review letters* **62**, 47 (1989).
- [31] A. Chabanov, M. Stoytchev, and A. Genack, *Nature* **404**, 850 (2000).
- [32] P. W. Anderson, *Physical Review* **109**, 1492 (1958).
- [33] I. Kolokolov, V. Lebedev, and P. M. Lushnikov, *Physical Review E* **101**, 042137 (2020).
- [34] D. G. Voelz, (No Title) , 51 (2011).
- [35] R. L. Phillips and L. C. Andrews, *Journal of the Optical Society of America* **71**, 1440 (1981).
- [36] J. Garnier and K. Sølna, *Journal of the Optical Society of America A* **39**, 1309 (2022).
- [37] J. Garnier, A. Picozzi, and T. Torres, *Physical Review Letters* **134**, 223803 (2025).
- [38] D. Voelz, E. Wijerathna, A. Muschinski, and X. Xiao, *Optical Engineering* **57**, 104102 (2018).
- [39] S. Malekpour, J. A. Gubner, and W. A. Sethares, *Journal of the Franklin Institute* **355**, 2932 (2018).
- [40] G. Carter, C. Knapp, and A. Nuttall, *IEEE transactions on audio and electroacoustics* **21**, 337 (2003).
- [41] D. S. Wiersma, P. Bartolini, A. Lagendijk, and R. Righini, *Nature* **390**, 671 (1997).
- [42] T. Schwartz, G. Bartal, S. Fishman, and M. Segev, *Nature* **446**, 52 (2007).
- [43] L. B. Stotts and L. C. Andrews, *Optical Engineering* **63**, 041207 (2024).
- [44] A. Nair, Q. Li, and S. N. Stechmann, *Optics Letters* **48**, 3865 (2023).
- [45] G. Bal and A. Nair, *Waves in Random and Complex Media* , 1 (2025).
- [46] B. E. Saleh and M. C. Teich, *Fundamentals of photonics, 2 volume set* (John Wiley & Sons, 2019).